Effects of column density on I2 spectroscopy and a determination of I2 absorption cross section at 500 nm

P. Spietz, J. C. Gómez Martín, J. P. Burrows

Atmos. Chem. Phys. Discuss., 5, 5183–5221, 2005
www.atmos-chem-phys.org/acpd/5/5183/
SRef-ID: 1680-7375/acpd/2005-5-5183
European Geosciences Union

Atmospheric Chemistry and Physics Discussions

Effects of column density on I_2 spectroscopy and a determination of I_2 absorption cross section at 500 nm

P. Spietz, J. C. Gómez Martín, and J. P. Burrows

Institute of Environmental Physics (IUP), University of Bremen, PO Box 330440, 28334 Bremen, Germany

Received: 15 March 2005 – Accepted: 27 June 2005 – Published: 22 July 2005

Correspondence to: P. Spietz (peterspietz@iup.physik.uni-bremen.de)

Abstract

The use of ro-vibronic spectra of I_2 in the region of 543 nm to 578 nm as reference spectra for atmospheric Differential Optical Absorption Spectroscopy is studied. In this study it is shown that the retrieval of atmospheric column densities with Differential Optical Absorption Spectroscopy set-ups at FWHM at and above 1 nm depends critically on the column density, under which the used reference spectrum was recorded. Systematic overestimation of the comparatively low atmospheric column density of I_2 of the order of 13% is possible. Under low pressure conditions relevant in laboratory studies, the systematic deviations may grow up to 45%. To avoid such effects with respect to field measurements, new reference spectra of I_2 were determined under column density of the order of 10^{16} molec/cm^2 close to that expected for the atmospheric measurement. Thereby the described systematic deviations are avoided. Two typical configurations of Differential Optical Absorption Spectroscopy, which use grating spectrometers, were chosen for the spectroscopic set-up. One spectrum was recorded at similar resolution (0.25 nm FWHM) but finer binning (0.035 nm/pixel) than previously published data. For the other (0.59 nm FWHM, 0.154 nm/pixel) no previously published spectra exist. Wavelength calibration is accurate to ±0.04 nm and ±0.11 nm respectively. The absorption cross section for the recordings was determined under low column density with an accuracy of ±4% and ±3% respectively. The absolute absorption cross section of I_2 at 500 nm (in standard air) in the continuum absorption region was determined using a method independent of iodine vapour pressure. Obtained was $\sigma_{I_2}(500\,\text{nm})=(2.186\pm0.021)\cdot10^{-18}\,\text{cm}^2\cdot\text{molec}^{-1}$ in very good agreement with previously published results, but at 50% smaller uncertainty. From this and previously published results a weighted average of $\sigma_{I_2}(500\,\text{nm})=(2.191\pm0.02)\cdot10^{-18}\,\text{cm}^2\cdot\text{molec}^{-1}$ is determined.

ACPD

5, 5183–5221, 2005

1. Introduction

Descriptions of resolution related issues in the ro-vibronic spectrum of I_2 have been reported frequently in the past. Vogt and Koenigsberger (1923) studied the extinction coefficient of iodine vapour in the visible and infrared. They observed strong variation of extinction with temperature, I_2 concentration[1] and foreign gas pressure and reported a clear non-linear behaviour of extinction with respect to concentration – i.e. a deviation from Beer-Lambert's law. Rabinowitch and Wood (1936) determined the transition region between the continuous part of the spectrum below 500 nm and the structured part above 500 nm by varying foreign gas pressure. This left the continuous part of the spectrum unchanged while the structured part changed its apparent extinction significantly. They distinguished clearly between changes due to unresolved rotational lines and effects caused by pressure induced line broadening. Kortüm and Friedmann (1947) recorded the banded region at moderate resolution, relating the observed structure also to the unresolved rotational lines. They also distinguished between pressure induced and concentration induced changes in observed extinction. Ogryzlo and Thomas (1965) proved that the observed "pressure" dependence of the I_2 absorption spectrum above 500 nm indeed results from pressure broadening of the rotational lines. Tellinghuisen (1973) thoroughly studied the extinction coefficient of I_2 in the visible and NIR under low resolution and resolved the observed spectrum into three transitions $A(^3\Pi_{1u})\leftarrow X(^1\Sigma_{0g+})$, $C(^1\Pi_{1u})\leftarrow X(^1\Sigma_{0g+})$, and $B(^3\Pi_{0u+})\leftarrow X(^1\Sigma_{0g+})$ (see Gray et al., 2001, for labelling of transitions). Today the ro-vibronic spectrum of I_2 is well documented by high-resolution measurements (Gerstenkorn and Luc, 1977a, b, 1978; Gerstenkorn et al., 1982; Kato et al., 2000) and I_2 absorption lines are used as easily accessible wavelength calibration standards (e.g. Marcy and Butler, 1992).

[1] In some publications the misleading wording "pressure dependence of the I_2 spectrum" was used when relating to I_2 concentration. In the absence of bath gas, $[I_2]$ was varied by varying temperature and thereby vapour pressure. This should not be mixed up with "pressure dependence" resulting from the presence of a foreign gas.

ACPD
5, 5183–5221, 2005

But quantitative spectroscopy of I_2 in the said region and under low resolution conditions is still difficult. Because of unresolved ro-vibronic structure each low-resolution spectroscopic measurement is dominated by instrumental artefacts. Due to that, optical density (OD) is not linear in concentration, if calculated by applying Beer-Lambert's law directly to detector outputs recorded under such conditions. Quantitative spectroscopy, which uses low-resolution laboratory spectra of I_2 as reference data, is limited if not impeded by this. Interest in suitable reference spectra of I_2 covering the ro-vibronic region arose (Saiz-Lopez et al., 2004) after the observation of considerable amounts of I_2 in Differential Optical Absorption Spectroscopy measurements (DOAS, see e.g. Finlayson-Pitts and Pitts, 2000, and Solomon et al., 1987, on zenith sky absorption measurements) in the marine boundary layer at Mace Head, Ireland (Saiz-Lopez and Plane, 2004).

With respect to the absorption cross section of I_2 at 500 nm, i.e. outside the ro-vibronic region, a number of studies had been performed in the past. The first determination of the extinction coefficient of I_2 had been performed by Vogt and Koenigsberger (1923). Other quantitative studies followed by Rabinowitch and Wood (1935), Kortüm and Friedheim (1947), Sulzer and Wieland (1952), and Tellinghuisen (1973) establishing the latter's result for the cross section as the most reliable one. The recent observation of I_2 in the marine boundary layer by Saiz-Lopez and Plane initiated further studies on the absorption cross section. Studies by Saiz-Lopez et al. (2004) as well as previously unpublished results by Bauer et al. (2004) followed. In recent laboratory studies on the determination of absorption cross sections of iodine oxides as well as related kinetics studies (e.g. EU Framework 5 Program THALOZ) the knowledge of the absorption cross section of I_2 is an important prerequisite to any quantitative analysis adding further to the newly increased interest in I_2.

Both issues, quantitative spectroscopy for DOAS with typical low resolution and the absolute absorption cross section of I_2 at 500 nm are being addressed in this work.

2. Reference spectra of I_2 for DOAS

Due to the measurement process performed with a moderately resolving spectrometer and a semi-conductor detector array, any measurement of unresolved rotational lines will be dominated by instrumental artefacts. The reason for this is the unresolved irregular distribution and mixing of strongly absorbing and absorption free spectral sections within the low-resolution recording. The instrumental artefacts will be a non-linear function of column density (the product of geometric path length and concentration). Likewise such measurements are prone to contain "saturated" rotational lines, i.e. lines which are too strong to allow any measurable intensity to pass at their specific wavelength. This is especially true of laboratory measurements in which it is tempting to use optical densities of the order of 0.5 to 1.0 to improve the signal to noise ratio. Already at I_2 vapour pressure (room temperature) and a path length of 10 cm a large number of I_2 rotational lines between 510 nm and 560 nm are at optical densities above 3. If optical density is calculated by applying the Beer-Lambert law directly to the detector output of measured intensities, an "apparent" optical density A_{app} will be obtained, which is not linear in concentration. Figure 1 shows two spectra recorded at significantly different column densities under otherwise constant conditions. Resolution was low and rotational lines were far from being resolved. In the continuum range below 500 nm the low column density spectrum is scaled to the high column density one. In the ro-vibrational region the apparent optical density A_{app} clearly grows sub-linearly with column density. Opposed to that optical density at and below 500 nm is continuous and therefore perfectly linear in column density.

In the following Sect. 2.1 firstly the effect of resolution and binning on low-resolution recordings of the I_2 ro-vibronic spectrum will be studied. As a consequence from the findings in the simulation section new reference spectra for I_2 were recorded to be used in atmospheric DOAS retrieval. The experiments and the analysis leading to these new reference spectra are presented in Sect. 2.2.

2.1. Simulations

To determine the possible effect of low resolution and coarse binning on quantitative spectroscopy, spectra were simulated based on a high-resolution spectrum of I_2 obtained with a Fourier Transform Spectrometer (FTS), courtesy of Marcy and Butler (1992). Conditions for this high-resolution spectrum are specified as signal to noise S/N=1000, resolution $\lambda/\Delta\lambda$=400 000 ($\approx$0.04 cm^{-1}), [I_2] at vapour pressure (room temperature) without bath gas and 10cm optical path. A section of this spectrum is shown in the inset graph of Fig. 1. Clearly a considerable number of lines already reaches OD of the order of 2 to 3. In the lack of other high-resolution data recorded under lower OD and given the large signal to noise ratio of that measurement, this spectrum was nevertheless used as the "true" spectrum in our simulations. The spectrum was convoluted with a 0.3 cm^{-1} Lorentz profile to simulate atmospheric pressure broadening. This curve is also shown in the inset graph of Fig. 1. An FTS recording of a Xenon lamp obtained at 2 cm^{-1} resolution was interpolated onto the grid of the I_2 spectrum to be used as the reference intensity $I_0(\lambda)$. These three data sets were then used to simulate low resolution and coarsely binned apparent optical densities A_{app} under different spectroscopic conditions. To this end the high-resolution I_2 absorption spectra (low pressure and pressure broadened) were scaled to different amplitudes simulating differently strong "true" optical densities $A_i(\lambda)$. Scaling took the change in peak height into account, which is caused by pressure broadening. Thereby quantitative comparability was maintained. Applying the Beer-Lambert law, the different absorption measurements $I_i(\lambda)$ were simulated:

$$I_i(\lambda) = I_0(\lambda) \cdot \exp[-A_i(\lambda)] \quad (1)$$

Limited resolution of the spectrometer was simulated by convoluting both $I_i(\lambda)$ and $I_0(\lambda)$ with a gaussian shaped instrument's characteristic function $S(\lambda)$. The resulting $I_{c,i}(\lambda)$ and $I_{c,0}(\lambda)$ were then binned (numerically integrated) onto a grid of pixels of fixed size (continuous $\lambda \rightarrow$discrete j) and from the binned signals $I_{c,i}$(j) and $I_{c,0}$(j) an "apparent"

ACPD
5, 5183–5221, 2005

optical density $A_{app,i}$(j) was calculated:

$$A_{app,i}(j) = \ln\left(\frac{I_{c,0}(j)}{I_{c,i}(j)}\right) = \ln\left(\frac{\int_{\lambda_j}^{\lambda_{j+1}}\int_{-\infty}^{+\infty} S(u)\cdot I_0(\lambda-u)\,du\cdot d\lambda}{\int_{\lambda_j}^{\lambda_{j+1}}\int_{-\infty}^{+\infty} S(u)\cdot I_0(\lambda-u)\cdot\exp(-A_i(\lambda-u))\,du\cdot d\lambda}\right) \quad (2)$$

This use of apparent optical density is the same as in the study by Tellinghuisen (1973), who tackled the problem in terms of apparent extinction. For our simulations we choose spectroscopic conditions, which correspond to typical DOAS configurations (Roscoe et al., 1999, and references therein), see Table 1.

The peak amplitude of true optical density $A_i(\lambda)$ was varied such that it covered the range from ≈0.004 to 1.4 in units of equivalent optical densities A(500 nm) relevant for field (low end, compare Saiz-Lopez and Plane, 2004) and lab (high end). For comparison, room temperature saturated vapour pressure of I_2 at 50 cm path length produces an optical density of ≈1.1 at 500 nm.

2.1.1. Results from simulated data

The comparison of the simulated spectra showed that the pressure broadened spectra grow faster in apparent OD than do the low pressure spectra, perfectly in line with the observations of e.g. Rabinowitch and Wood (1935). The increase is caused by redistribution of absorption from the line centres to the gaps between lines, compare Fig. 1. Thereby absorption at atmospheric pressure contributes across the full width of the detector's pixels instead of – as in the low pressure spectrum – only at the line width, which is narrow in comparison to the detector's pixel. The same as for apparent OD as such is also true for the amplitude of differential structures in the apparent OD spectrum, see Fig. 2a and b.

To detect any non-linear behaviour of the resulting apparent OD with respect to concentration or rather column density (i.e. the product of concentration and path length), there exist two different possibilities of representation. One is to plot apparent OD at a selected wavelength against true OD, which was initially fed into the model. But with respect to application it is more illustrative to choose an equivalent OD at 500 nm as independent variable. Equivalent OD at 500 nm is abbreviated as A(500 nm) and is obtained by transferring the true OD which was originally fed into the model from its wavelength λ_T>500 nm to 500 nm, where an empirical ratio between the cross sections at 500 nm and that at wavelength λ_T of the initial true OD is used. This is indeed equivalent, as OD at 500 nm in contrast to that at λ>500 nm is linear in column density. The other possibility is to normalise apparent OD to column density (or any other quantity proportional to it) and check, whether the normalised result is "constant". Both types of representation will be used below.

As DOAS relies upon "differential" spectra of apparent OD – designated by $\Delta A_{app}(\lambda)$ –, these were extracted by subtracting a suitable slowly varying polynomial from $A_{app}(\lambda)$, see e.g. Finlayson-Pitts and Pitts (2000), Solomon et al. (1987) and then normalising the resulting $\Delta A_{app}(\lambda)$ to equivalent OD at 500 nm. In the absence of non-linear effects the normalised differential spectra $\Delta A_{app}(\lambda)$/A(500 nm) should be directly proportional to differential cross section and should therefore be the same for all different OD. The results for a selected band (546 nm) are shown in Fig. 2a for a 1200 grooves·mm^{-1} grating at 0.175 nm FWHM and in Fig. 2b for a 300 grooves·mm^{-1} grating at 1.3 nm FWHM, both being currently used DOAS configurations. They are clearly not constant with column density, even though the effect is smaller in the pressure broadened case. The deviation from constant behaviour was quantified by firstly measuring the amplitude of differential structure from valley to peak. This amplitude was then plotted against equivalent OD at 500 nm, designated by A(500 nm) (Fig. 3). Comparison of the two cases of A(500 nm)≈0.01 and A(500 nm)≈1.0, which are representative values for field and lab respectively, yields the relative difference. The selected lower equivalent OD of A(500 nm)≈0.01 corresponds to the order of magnitude

of an atmospheric column density observed at the 8.4 km long path DOAS measurement reported by Saiz-Lopez and Plane (2004). The larger one of ≈1.0 to a typical laboratory measurement at room temperature and saturated vapour pressure of I_2 and 50 cm path length.

Both at low as well as at atmospheric pressure the amplitude of apparent differential cross section is noticeably reduced by increasing column density. If a high column density reference spectrum from the lab were used for DOAS retrieval of low column densities, the column density would be overestimated correspondingly. In the pressure broadened atmospheric case overestimation amounts to 2%, 12% and 13% for 1200 grooves·mm^{-1}, 0.175 nm FWHM (filled squares), 600 grooves·mm^{-1}, 1.0 nm FWHM (filled circles) and 300 grooves·mm^{-1}, 1.3 nm FWHM (filled triangles) respectively. In the low pressure case overestimation reaches 45% and is quite independent of spectroscopic conditions. Use of DOAS in low pressure laboratory studies therefore requires great care in selecting an appropriate reference spectrum. A simulation for 600 grooves·mm^{-1}, 0.35nm FWHM (Fig. 3, pressure broadened case, open circles) was also preformed to examine the source of the observed effect. Here it is helpful to consider the spectral width $\Delta\lambda$ of pixels in different configurations. Spectral width we define as the spectral interval covered by a single pixel for a given grating and spectrometer. For the performed simulations the values are listed in Table 1. The ratio of FWHM and spectral width $\Delta\lambda$ defines, how many pixels cover the FWHM interval. Comparing the ratio of FWHM upon $\Delta\lambda$ to the observed effect on ΔA_{app} shows that not binning – i.e. the number of pixels covering a spectral feature – but resolution expressed by FWHM is the major source of the effect. This result can give an orientation what to expect, but it can not be generalised, as the effect on ΔA_{app} is not the same in each band, see Fig. 4. There reduction of ΔA_{app} is plotted for three different bands (542 nm, 544 nm, and 546 nm). Note the partially mixed order of curves indicating differently strong and partially reversed effects for different spectroscopic conditions. This different behaviour of ΔA_{app} in different bands presents a further problem, if reference spectra recorded at high column density – i.e. high A(500 nm) – were to be used for

DOAS retrieval of low atmospheric column densities.

The fact that at low pressure deviation in ΔA_{app} is quite independent of spectroscopic conditions indicates that here it is most likely caused by largely varying intensity across the spectral width of pixels. Strong rotational lines are mixed with gaps between them, which are practically free of absorption, compare inset graph in Fig. 1. Saturation of unresolved rotational also plays a role in this, as peak absorption in isolated rotational lines reaches OD of the order of 1.1 already at equivalent OD of A(500 nm)≈0.1.

The found overestimation can be minimised by using reference spectra recorded in the range of column density expected in the DOAS application. In this context it has to be kept in mind that the observed effects are also instrument dependent, where instrument characteristics entered into the simulation via the instrument's characteristic function $S(\lambda)$ and the pixel size used for numeric integration (binning).

Therefore the best approach is to dedicatedly measure I_2 reference spectra with the DOAS instrument itself in the lab at a column density which is similar to those expected in the atmosphere. If the DOAS instrument itself cannot be used, the second best solution is to use a spectrometer and detector of same type and under the same spectroscopic conditions (grating, slit width) as later in the atmospheric measurement. In this sense – given the available equipment in our lab – the spectra presented below were measured. With the two aspects "spectroscopic conditions" and "atmospheric target column density" taken into account, overestimation introduced by insufficient resolution will be minimised to 1% or even less, see Fig. 3.

2.1.2. Method for largely varying column densities

If an absorber's apparent spectrum should display significant variation already on the scale of column densities expected in the atmosphere (which is not the case for I_2), a single reference spectrum "centred" in the middle of the expected range does not suffice. Rather the expected range of column density has to be covered by a "set of reference spectra" valid for column densities $C_{I_2,j}$. For the corresponding differential apparent reference spectra $\Delta A_{app}(\lambda, C_{I_2,j})$ a polynomial can be determined at each

wavelength λ to interpolate apparent reference spectra for each possible intermediate column density C_{I_2}:

$$\Delta A_{app}\left(\lambda, C_{I_2}\right) = \sum_{k=0}^{m} a_k(\lambda) \cdot C_{I_2}^k \quad (3)$$

The variable of this polynomial is column density C_{I_2}. The coefficients $a_k(\lambda)$ are determined to fit the discrete set of $\Delta A_{app}(\lambda, C_{I_2,j})$ at each wavelength. Instead of a simple differential reference spectrum $\Delta\sigma_{app,I_2}(\lambda)$ valid for a given instrument and at the chosen target column density now the wavelength dependent coefficients contain the information about the reference spectrum plus the instrumental and concentration dependent effects.

2.2. Measurement of reference spectra

To obtain I_2 reference spectra for DOAS, absorption spectra were measured at 1000 mbar (N_2 grade 4.8 added) with the set-up described below. The only difference was in that measurements were performed in flow mode using a different iodine reservoir. This enabled either a flow of N_2 through the iodine reservoir or bypassing it. Thereby pressure and flow in the vessel could be maintained constant between reference intensity and absorption intensity measurements with only the iodine being "switched on" or "off". Two spectroscopic configurations were used: Firstly a 300 grooves·mm^{-1} grating and 50 μm slit width ($\rightarrow$0.59 nm FWHM, 0.154 nm/pixel) covering the interval from 445 nm to 600 nm. This enabled direct determination of apparent cross section in the ro-vibronic range, as the continuous part of the absorption at 500 nm could be used for determination of concentration. At 500 nm the absolute absorption cross section of $\sigma_{I_2}(500\,\text{nm})=(2.19\pm0.02)\,\text{cm}^2\cdot\text{molec}^{-1}$ determined in this work (see below) was used.

A second reference spectrum was recorded with a 1200 grooves·mm^{-1} grating and 170 μm entrance slit ($\rightarrow$0.25 nm FWHM, 0.035 nm/pixe) covering the range from

543 nm to 578 nm (560 nm centre wavelength). This corresponded to the conditions in Saiz-Lopez and Plane (2004). There, atmospheric measurements were made with an identical spectrometer as in this study (Acton Research 500 mm Czerny-Turner spectrograph). With the narrow spectral window of the 1200 grooves·mm^{-1} grating absolute calibration of apparent differential cross section was achieved by additional measurements before (index "b") and after (index "a"). These determined concentration at 500 nm in the continuous part of the spectrum. During the three absorption measurements of $I_{500\,nm,b}(\lambda)$, $I_{560\,nm}(\lambda)$, and $I_{500\,nm,a}(\lambda)$ concentration of $[I_2]$ was maintained constant in the vessel. Therefore between the intensity reference $I_{0,560\,nm,b}(\lambda)$ and the middle measurement $I_{560\,nm}(\lambda)$ the spectrometer had to be moved for the 500 nm measurement block. The same holds for $I_{0,560\,nm,a}(\lambda)$. Errors due to this were negligible, because the uncertainty in reproducibility of spectrometer position was better than 0.03 nm. This is small with respect to the – in the region 543 nm to 578 nm – smooth and only slowly varying spectrum of the Xenon arc lamp, which was used in these experiments. By the procedure described above, absolute calibration of concentration was transferred from 500 nm to the apparent optical density spectra in the structured region.

Wavelength calibration was obtained by recording the emission spectrum of a line source (Platinum-Chromium-Neon and Mercury-Cadmium). Calibration was checked and improved by calibrating the measured spectrum against the convoluted high-resolution FTS spectrum from Marcy and Butler. This had a wavelength accuracy of better than 0.001 nm (corresponding to 0.04 cm^{-1} resolution as upper limit of wavelength accuracy). In the calibration of the I_2 spectrum measured with the 1200 grooves·mm^{-1} grating, eight band maxima of I_2 distributed evenly across the spectral range were used. The mean error of calibration ranged between 0.02 nm and 0.04 nm setting the uncertainty to ±0.04 nm. The same procedure was used for the measurement recorded with the 300 grooves·mm^{-1} grating. 33 band maxima distributed across the interval from 510 to 580 nm were used. The mean error of calibration ranged between 0.03 nm and 0.11 nm setting the uncertainty to ±0.11 nm. FWHM

was determined from the apparent shape of isolated emission lines from the mercury-cadmium line source.

2.2.1. Resulting spectra

The I_2 reference spectrum obtained for the 1200 grooves·mm^{-1} measurement is shown in Fig. 5a. Also shown are the artificial, pressure broadened, convoluted and binned spectrum based on the FTS data from Marcy and Butler (1992) and the FTS spectrum measured by Saiz-Lopez et al. (2004). For comparability the latter is scaled at 500 nm to the cross section of (2.19±0.02)·10^{-18} cm^2·molec^{-1} as determined and used in this work. To our best knowledge the spectrum of Saiz-Lopez at al. is the only other I_2 reference spectrum published for use in DOAS.

Transfer of concentration from 500 nm to the spectral range of the reference spectrum could be accomplished with an uncertainty of about 4%. This estimate was obtained by comparing empty vessel measurements "before" and "after". This gave a measure for the possible presence of deposit on the windows. Comparison of spectra obtained from different series of spectra confirmed this uncertainty estimate. The signal to noise in our grating spectrum is of the order of 1:70 determined from the ratio of two independent measurements.

In the centre region around 562 nm all three spectra coincide well, compare the ratios of spectra, top graph of Fig. 5a. But the general pattern of ratios shows also that this region represents a turning point as to the blue side the convoluted spectrum falls low (ratio>1) while the FTS spectrum falls high with respect to our spectrum (ratio<1). To the red side the order is reversed. In the centre at 560 nm occurs a step in the ratio with the FTS spectrum by Saiz-Lopez, while the ratio with the convoluted and binned Marcy and Butler spectrum continues smoothly.

The differential structure in the ratio with the Saiz-Lopez spectrum is surprisingly different in the two halves of the considered interval changing abruptly with the step at the centre. The differential structure in the other ratio develops smoothly from the red increasing to the blue. Band correlated structures in the ratio between our grating

spectrum and the FTS spectrum by Saiz-Lopez coincide clearly with the steep blue flank of the bands. They show deviations at the bottom as well as at the top of the flanks ranging from a few percent up to 10%. The direction of deviation changes quite systematically.

Effects of step size (0.1 nm) are clearly visible in the FTS spectrum by Saiz-Lopez, where band heads are levelled off and flanks appear bent and irregular (picket-fence effect). The grating spectrum displays regular flanks and clear band heads, in general agreeing accurately with the shapes in the convoluted FTS spectrum of Marcy and Butler. There exist some discrepancies in shape between our grating spectrum and the convoluted Marcy and Butler spectrum, but the shape and amplitude of the bands in general is in good agreement.

In Fig. 5b the spectrum obtained with a grating of 300 grooves·mm^{-1} is shown. No transfer of calibration was necessary, as λ=500 nm was included in the spectral interval. Three series of at least 10 spectra each were recorded. Effects of deposit on the windows were corrected. The scatter between the spectra was of the order of a few percent, which is negligible with respect to non-linear effects in OD. Therefore all were scaled at 500 nm to the I_2 cross section determined below. After that they showed a 2.5% scatter in the differential structure between 540 and 560 nm. Along with the uncertainty in the used cross section of 1% this defines the uncertainty in the apparent cross section spectrum to conservatively estimated 3%. Signal to noise was determined in the continuum range below 500 nm to be of the order of 1:50.

The ratio between the 300 grooves·mm^{-1} spectrum and the FTS spectrum by Saiz-Lopez et al. (2004) shows the same general pattern as the ratio of the 1200 grooves·mm^{-1} grating spectrum and their FTS spectrum. Different behaviour in the two halves of the spectral window as well as a step at the centre are present. Band correlated structures of ≈10% are significantly larger and at the same positions as above. The downward peaks in the ratio coincide with the bottoms of the steep blue flanks.

2.3. Discussion and conclusion

The inclination of ratios could in principle be caused by a vertical offset of one of the spectra. But in that case the ratio should not intersect with a horizontal at 1.0 as in the present case. It is interesting to note that to the blue side of 560 nm – near the observed turning point of 562nm – the $C(^1\Pi_{1u}) \leftarrow X(^1\Sigma_{0g+})$ and $B(^3\Pi_{0u+}) \leftarrow X(^1\Sigma_{0g+})$ transitions are relevant while to the red of 560 nm the $A(^3\Pi_{1u}) \leftarrow X(^1\Sigma_{0g+})$ becomes dominant (compare Tellinghuisen, 1973, and Gray et al., 2001). This explains the inclination with respect to the convoluted Marcy and Butler FTS spectrum. This was obtained from a sole absorption measurement. An intensity reference measurement was not performed, as this is not needed in the context of their application. To calculate OD, we simulated an intensity reference by fitting a smooth curve above the dense structure of absorption lines following the clearly visible envelope of intensity. This is justified as long as the absorption lines are narrow with gaps of zero absorption between them. Any smooth continuum absorption will be lost by this approximation. Due to that the $C(^1\Pi_{1u}) \leftarrow X(^1\Sigma_{0g+})$ continuum absorption is not present in our artificial OD of the Marcy and Butler FTS spectrum. Therefore at wavelength below approx. 580 nm the convoluted Marcy and Butler spectrum as simulated in this work has to fall below any spectrum obtained with a real intensity reference. The reversed behaviour above 560 nm could be caused by inaccurate scaling of the convoluted Marcy and Butler spectrum. Absolute scaling was obtained by varying the peak value of assumed "true" OD such, that the convoluted and binned spectrum reproduced the differential amplitude of our measured spectrum between 550 and 560 nm. The scaling region covers the centre region exactly, where the ratio intersects the horizontal at 1.0. An overestimation of the iteratively and only roughly – because otherwise irrelevant – determined relative scaling of the order of 15% directly produces an underestimation in the ratio, as observed.

The deviations in the ratio between our spectrum and that by Saiz-Lopez et al. (2004) are less easily understood. It is important to note, that the general pattern of the ra-

tio is the same for the 1200 grooves·mm^{-1} and the 300 grooves·mm^{-1} grating, which were obtained in different sets of experiments. At first sight such different behaviour in both halves of the spectral interval and the steep step at the centre could indicate a – for technical reasons necessary – joining of different sections of FTS recordings. But this is not the case for the spectrum by Saiz-Lopez et al. (2004), where different sections were joined by linear weighting. The overlap region in the visible ranged from 500 to 555 nm. The column density in the recording of the FTS spectrum was $3.1{\cdot}10^{16}$molec·cm^{-2} (Saiz-Lopez, private communication), which is only a factor of 5 larger than in our recording with the 1200 grooves·mm^{-1} spectrum. There column density was $(6.86{\pm}0.20){\cdot}10^{15}$ molec· cm^{-2}. This and the general shape and the magnitude of the discrepancy between their spectrum and ours clearly prove, that the discrepancies are not caused by column density dependent effects. Rather different resolution and possibly light source drift or deposit causing broad band changes of throughput are likely. The differential amplitude in the Saiz-Lopez spectrum is 30% larger than in our grating spectrum (see Figs. 5a and 6). Resolution in the FTS recording was stated to be 4 cm^{-1}, which at 550 nm corresponds to 0.12 nm. This is nearly the same as the chosen step size of 0.1 nm in their spectrum, explaining the observed picket-fence effect in their spectrum. A smaller step size would improve comparability and reduce the picket-fence effect. In our grating spectrometer recording FWHM was 0.25 nm. This is roughly a factor of two larger than in the FTS spectrum and could explain the observed larger differential amplitude.

The differential structure in the ratio between our spectrum and the convoluted FTS spectrum of Marcy and Butler follows the pattern of the ro-vibrational bands. The deviations are likely due to the simulation process, in which a gaussian shaped instrument's function had been used. This is a clear idealisation opposed to the true instrument's function of our spectrometer, which is irregularly shaped and asymmetric. Therefore the use of the experimentally determined FWHM for the gaussian shaped convolution kernel can only be an approximation. This would distort the band shape especially at steep flanks. A similar argument holds for the artificial pressure broadening, in which

a Lorentz profile of idealised fixed width was used. Apart from that, strong and possibly saturated lines present in the original Marcy and Butler measurement could be responsible as well, see above and Fig. 1.

While comparability is somewhat limited by different resolution and step size, the presented spectra are in reasonable agreement with the FTS spectrum by Saiz-Lopez et al. (2004). Consistency of our measured and simulated spectra supports the validity of the conclusions drawn from the simulations. For measurements with 1200 grooves·mm^{-1} grating and FWHM of 0.175 nm no significant problems have to be expected from different column density. But in different spectroscopic configurations at low resolution, i.e. FWHM of 1.0 nm and above, the effects by different column density become significant. This justifies dedicated measurements of reference spectra at target column density and with the DOAS instrument itself or at least with the same type of instrument. The two absorption spectra presented in this work take both aspects into account. They were both measured under column densities of the order of 10^{16} molec/cm^3 which according to Saiz-Lopez and Plane (2004) is close to those expected in the atmosphere. Furthermore they were recorded under spectroscopic conditions which are typical for currently used DOAS configurations. Both spectra are available as supplementary data to this publication (http://www.atmos-chem-phys.org/acpd/5/5183/acpd-5-5183-sp.zip).

3. Absorption cross section of I_2 at 500 nm

3.1. Experimental set-up

A schematic diagram of the set-up is shown in Fig. 7. It comprises a reaction vessel, a grating spectrometer, and a CCD camera (charge-coupled device) as detection system. The reaction vessel is made of glass and has no thermal insulation or stabilisation. Experiments were performed at room temperature. The length of the vessel was (26.4±0.2) cm. This was the shortest vessel available, thus enabling higher

iodine concentrations without too large optical densities. Larger concentrations enabled more accurate measurement of pressure. To avoid I_2 condensation, the partial pressure was always kept below saturated vapour pressure. The optical windows of the vessel are made from fused silica (50 mmm dia.). A 150 W Xenon arc lamp (Hamamatsu) was used as light source for absorption spectroscopy. After having traversed the vessel, the analysis light was directed into a Czerny-Turner spectrometer (Acton Research, 500 mm focal length) operated alternatively with one of three different gratings (1200 grooves·mm^{-1} holographic, 300 grooves·mm^{-1} and 150 grooves·mm^{-1}, both blazed at 300 nm).Spectra were recorded with a CCD camera (Roper Scientific) with a 1024×1024 silicon detector chip (0.26 μm pixel width, SiTE). To enable monitoring of the light source during absorption measurements and thus to account for possible light source drift, a second beam of light was passed parallel to the vessel. With a flip mirror the light was directed either via the vessel or directly from the light source towards the spectrometer.

Pressure in the vessel was the crucial parameter in the determination of concentration. Therefore it was measured using a temperature stabilised capacitance pressure transducer (MKS Baratron 627B) with 0.001 to 1 mbar range, allowing for high linearity, low hysteresis and reproducibility of the pressure readings (specified ±0.12% of reading). For recording spectra at atmospheric pressure a capacitance pressure transducer of 1100 mbar maximum range was also connected. Zero point correction was performed with a Penning type pressure head (Edwards, 10^{-3} to 10^{-7} mbar).The temperature of the gas in the vessel, ambient temperature and the temperature of the reservoir were all measured with calibrated 3 wire Pt 100 temperature sensors. The manufacturer's specification for the sensors is ±0.07 K. The transducers were calibrated and specified to the same accuracy of ±0.07 K. As a conservative error estimate for temperature measurement 0.5 K was assumed based on a comparative measurement. The vessel was connected to a reservoir, where the iodine was maintained. The pressure in the reservoir was monitored with the same type of temperature stabilised and high accuracy capacitance pressure transducer as the one connected to the ves-

sel, but with 0.01 to 10 mbar range. Pressure heads, vessel and iodine reservoir were connected to the vacuum pump such that all could be evacuated independently of each other. During all experiments pressure and temperature readings from all sensors were automatically recorded in sufficiently short time intervals to cover any changes accurately. The I_2, resublimed p.a., was obtained from ACROS Organics, C.A.S No.: 7553-56-2.

3.2. Determination of the absorption cross section of I_2

The absorption cross section was determined by simultaneously determining optical density via spectroscopic measurement and concentration via pressure and temperature measurement including careful leak rate correction.

3.2.1. Spectroscopic measurements

Each spectroscopic measurement consisted of a recording of the detector's dark signal, followed by repeated alternating measurements of the light source directly and through the vessel respectively. "Vessel" measurement and "direct" measurement consisted each of a fixed number of accumulations. By the alternating measurement procedure a near-simultaneous recording of both was achieved which enabled a highly effective correction of possible light source drift. Prior to each measurement series the accuracy of drift correction was verified by a set of such measurements without gas in the vessel. In a preparatory experiment within half an hour a light source drift occurred with a trend of the order of 0.02/h to 0.03/h plus irregular scatter of ±0.005, all in units of optical density. The drift was deliberately forced by irregularly venting the xenon arc lamp to create "worst case conditions" for this test. By the described near-real time monitoring the long term drift could in all test measurements be corrected to an irregular scatter in the averaged optical densities of less than ±0.0025 in units of optical density (determined as the standard deviation across a corrected measurement of zero optical density). "Coloured" structures in the uncorrected optical density spectra

of empty vessel measurements (caused by light source drift) were to a high degree but not completely removed. As a conservative error estimate for the remaining drift effects an average of the typically found amplitude of the coloured structures of ±0.006 was used. The error of an original measurement was estimated in the sense of a maximum error as the sum of the determined standard deviation of a corrected empty vessel measurement plus the estimated error from drift. Both statements – scatter of ±0.0025 and ±0.006 conservatively estimated systematic drift – define the general maximum uncertainty of ±0.0085 of determined optical densities with respect to light source drift. Following the described approach, all reference – i.e. empty vessel – and absorption measurements – with I_2 – were performed. It is pointed out that accumulation of deposit on the vessel windows is not corrected by this approach. This is taken into account below.

Wavelength calibration was obtained from measurements of a mercury cadmium line source. Only isolated lines were used for wavelength calibration. Unresolved groups of neighbouring lines were rejected. Wavelength with respect to the 500 nm absorption cross section of I_2 is given in air. Note: Spectra in the previous section are given in vacuum wavelength for direct comparability with FTS (and other) spectroscopic measurements.

3.2.2. I_2-handling and measurement procedure

In separate preparatory measurements the leak rates of the empty reservoir and the vessel were determined to be 0.3 μbar·min^{-1} and 2.1 μbar·min^{-1} respectively. In both cases the increase of pressure with time, which was caused by the leak rate, always displayed a clear linear behaviour on the time scale of our measurements. A linear fit to the vessel's pressure readings covering a 4 h leak test resulted in a correlation coefficient of R^2=0.99998 between the data points and the linear fit. This justifies extrapolation of the leak rate on the time scale of our measurements.

Prior to each filling both the vessel and the I_2-reservoir containing solid I_2 were evacuated separately to remove any foreign gases due to remaining leaks. After evacuation

the reservoir was closed to allow the build-up of gas phase I_2. The vessel was also closed and a number of spectroscopic reference measurements (each a set of "vessel" and "direct" intensity measurements) were performed on the evacuated vessel, providing the error estimate for the spectroscopic measurements and also the 'empty vessel' reference for the determination of OD. Parallel to the empty vessel spectroscopic measurements the pressure in the vessel was monitored to check the leak rate of the vessel.

In the next step the I_2-reservoir was connected to allow the I_2-vapour to stream into the vessel. In general the filling proceeded initially through a fast burst resulting from the pressure gradient between the I_2-filled reservoir and the evacuated vessel. After that, filling proceeded significantly slower dominated by the speed of release from solid to gas phase in the reservoir, where the I_2 vapour was no longer in equilibrium with the solid phase. In the measurement the vessel was preferably filled using the faster initial burst. Thereby it was assured that the partial pressure of I_2 was always below the saturated vapour pressure and condensation of I_2 thereby minimised.

After filling, the reservoir was disconnected from the vessel and a number of simultaneous pressure readings and spectroscopic measurements were recorded. This filling and measurement procedure was repeated in several steps each time adding some more I_2 into the vessel to collect data for different concentrations. Overall pressures in the vessel were always below 0.7 mbar and well within the range of the 0.001 to 1 mbar pressure transducer. Partial pressure of I_2 was obtained by correcting the time series of overall pressures for leak rate. As justified above, changes in pressure due to leak rate could be assumed to be linear in time with the aforementioned rates. The temperature measurements enabled correction of temperature drifts and conversion to concentration. The partial pressure of I_2 in the vessel was always below 0.35 mbar. The vapour pressure of I_2 at 298 K is 0.40 mbar (Chase, 1998). Condensation on surfaces and windows was thereby minimised.

3.2.3. Analysis

In spite of the partial pressure of I_2 being below saturated vapour pressure, still wall loss of I_2 occurred in the vessel. It led to a slow but visible reduction of both partial pressure of I_2 as well as of optical density in the spectroscopic measurement. The correlation between both effects was high. Therefore wall loss is automatically compensated in our determination of σ_{I_2}. Nevertheless, due to wall loss also a measurable deposit built up on the windows which was spectroscopically observed. The absorptions of I_2 and deposit were separated by multiple multivariate linear regression of the observed time series of spectra using their different spectroscopic appearance. They were fitted against an average of observed time profiles containing dominantly the deposit's absorption (340 nm to 380 nm) and a time profile observed at 500 nm containing dominantly I_2. This approach produced two continuous, smooth and non negative separated spectra of I_2 and deposit. The fit itself was characterised by high correlation coefficients and residuals distributed normally. This proved the contribution of deposit at 500 nm to be negligible, while becoming increasingly important from 485 nm (worst case: 3% relative to optical density of I_2) on to the blue side of the spectrum (20% at 460 nm). Consequently the recordings at 500 nm can be safely regarded as free of deposit within less than 1% relative to the I_2 absorption. Furthermore, at and below 500 nm the spectrum of I_2 is smooth and free of rotational structure. OD calculated from the pixel outputs is free of instrumental artefacts related to resolution issues. Therefore the wavelength of 500 nm is well suited for the determination of σ_{I_2}. In the absence of technical imperfections the series of "pure" I_2 OD spectra should vary linearly with partial pressure, i.e. concentration of I_2. The proportionality factor at each wavelength – i.e. pixel – directly determines the sought-for absorption cross section at that wavelength.

Therefore the measured OD at 500 nm was plotted as a function of partial pressure, i.e. concentration. A linear fit with zero intercept for this OD versus concentration was then performed. This yields the cross section σ_{I_2} at 500 nm as the slope of the obtained

line.

3.2.4. Results for the absorption cross section of I_2

Figure 8 shows the obtained OD of one of the two performed measurement series as a function of concentration and the corresponding linear fit. OD is normalised to unit path length. Each data point is the average of 4 to 6 individual spectroscopic determinations of optical density recorded at a certain I_2 partial pressure. Each spectroscopic determination is the average of 50 individual accumulations of "vessel" and "direct" as described above. The high quality of both linear fits for the two series was expressed by correlation coefficients of R^2=0.99951 and 0.99846 respectively. In the linear regression the estimated uncertainties of both axes were taken into account (Press et al., 1986). The uncertainty of concentration was determined after correction of all systematic effects covered by measurement, i.e. leak rate and temperature drift. It therefore contains only the uncertainties of the pressure head and the temperature sensor as stated by the manufacturers after error-propagation. The uncertainty of optical density is based on the aforementioned maximum uncertainty of 0.0085 in units of optical density and that of the measured length of the vessel of (26.4±0.2) cm. Note that the uncertainty of 0.0085 is not yet normalised to unit path length.

The error estimate resulting from the linear regression contains both the uncertainty of the observational data "and" the scatter of the individual data points with respect to the linear fit. The estimates for the cross section $\sigma_{I_2}(500\,\text{nm})$ obtained from the two series of data are determined as $(2.194\pm0.010)\cdot10^{-18}\,\text{cm}^2\cdot\text{molec}^{-1}$ and $(2.158\pm0.018)\cdot10^{-18}\,\text{cm}^2\cdot\text{molec}^{-1}$, where the stated uncertainty is that resulting from the linear regression. Using the inverse squared error as weight, a weighted average was calculated from the two results, the error of which being determined by error propagation. This yields $(2.186\pm0.009)\cdot10^{-18}\,\text{cm}^2\cdot\text{molec}^{-1}$. Apart from that also the uncertainty in wavelength calibration has to be taken into account and – via the estimated derivative of the spectrum at 500 nm – converted into an uncertainty of absorp-

ACPD
5, 5183–5221, 2005

tion cross section. Assuming an uncertainty of one pixel in wavelength calibration the uncertainty in cross section amounts to $\pm 0.012\,cm^2 \cdot molec^{-1}$ which is again conservative, as the accuracy of wavelength calibration is of sub-pixel order. To obtain the final uncertainty of the determined cross section, this uncertainty is added to that obtained from the linear regression in the sense of a maximum error estimate yielding the final result of our experiments to be $\sigma_{I_2}(500\,nm) = (2.186 \pm 0.021) \cdot 10^{-18}\,cm^2 \cdot molec^{-1}$.

3.2.5. Discussion

The absorption cross section determined in this way is an original determination of cross section being independent of vapour pressure data. It agrees very well with the recently published results, which are shown in Table 2. The disagreement between different data is always well within the stated uncertainties. The determination of Bauer et al. (2004) was also independent of vapour pressure using an approach similar to ours. The careful and extensive study by Tellinghuisen (1973) used vapour pressure data by Stule (1961) and Shirley and Giauque (1959). Light source drift was compensated by a two beam optical arrangement with beam alternator. The study by Saiz-Lopez et al. (2004) also used vapour pressure reference data to determine the cross section, which they measured independently and which agrees well with the previously published data (Chase, 1998; Shirley and Giauque, 1959).

Based on the results listed in Table 2 a weighted average was calculated, which used the reciprocal squared errors of the individual results as weights:

$$\sigma_{I_2}(500\,nm) = (2.191 \pm 0.02) \cdot 10^{-18} cm^2 \cdot molec^{-1} \quad (4)$$

The error of the weighted mean was determined by error propagation. Stated is a 1σ-error.

4. Conclusions

In the context of atmospheric DOAS measurements of I_2 the effect of different column density in reference spectrum and atmospheric spectrum on the results of quantitative spectroscopy were studied. Used was the ro-vibronic spectrum of I_2 in the range of 540 nm to 580 nm. For different typical DOAS configurations the error was estimated, which has to be expected from using a high column density laboratory spectrum as reference spectrum for DOAS retrieval of low atmospheric column densities. The errors were found to depend in first place on limited resolution, i.e. large FWHM and only in second place on bin-size defined by the grating. For a 1200 grooves·mm^{-1} grating and 0.175 nm (close to the conditions in Saiz-Lopez and Plane, 2004) the effect proved to be minor at 2%. But for spectroscopic conditions, in which for other reasons FWHM is chosen to be larger at 1.0 nm and above (see Roscoe et al., 1999), it is non-negligible, leading in the case of I_2 to an overestimation of atmospheric column density of the order of 12 to 13%. For two typical DOAS spectroscopic configurations reference spectra were dedicatedly measured at low column densities similar to atmospheric values and with typical DOAS instrumental conditions. The spectra are available as supplementary data. For low pressure measurements overestimation of column density was found to reach as much as 45%. Use of DOAS in low pressure laboratory studies therefore requires great care in selecting appropriate reference spectra.

The absolute absorption cross section of I_2 at 500 nm in the continuum region was determined in an independent measurement. The result of $\sigma_{I_2}(500\,\text{nm})=(2.186\pm0.021)\cdot10^{-18}\,\text{cm}^2\cdot\text{molec}^{-1}$ agrees very well with previously published data and the uncertainty could be reduced by more than 50%. A weighted average of $\sigma_{I_2}(500\,\text{nm})=(2.191\pm0.02)\cdot10^{-18}\,\text{cm}^2\cdot\text{molec}^{-1}$ of the recent determinations is suggested as the best available estimate for the absorption cross section.

Acknowledgements. This work was partially funded by the German Space Agency DLR through its support of the SCIAMACHY project, the European Union, and by the University and the State of Bremen. This work is part of and facilitated by IGBP-IGAC and EU-ACCENT

Net work of Excellence. The authors wish to express their gratitude to J. Tellinghuisen for fruitful discussion and helpful suggestions after critical reading of our manuscript. The authors also want to thank A. Saiz-Lopez for helpful comments and suggestions.

References

Alliwell, S. R. and Jones, R. L.: Measurement of atmospheric NO_3, 1. Improved removal of water vapour absorption features in the analysis for NO_3, Geophys. Res. Lett., 23, 2585–2588, 1996.

Bauer, D., Ingham, T., and Crowley, J. N.: Interactive comment on "Absolute absorption cross section and photolysis rate of I_2" by A. Saiz-Lopez et al., Atmos. Chem. Phys. Discuss., 4, S741–S743, 2004.

Chase Jr., M. W.: NIST JANAF Thermodynamical Tables, 4th edition, J. Phys. Chem. Ref., Monograph 9, 1998.

Finlayson-Pitts, B. J. and Pitts Jr., J. N.: Chemistry of the Upper and Lower Atmosphere, Academic Press, New York, 2000.

Gray, R. I., Luckett, K. M., and Tellinghuisen, J.: Component Analysis of the Visible Absorption Spectra of I_2 and Br_2 in Inert Solvents: Critique of Band Decomposition by Least-Squares Fitting, J. Phys. Chem. A, 105, 11 183–11 191, 2001.

Gerstenkorn, S. and Luc, P.: Atlas du spectre d'absorption de la molecule d'iode: 15.600–17.600 cm^{-1}, Laboratoire Aimé Cotton, CNRS II, 91405 Orsay, France, 1977a.

Gerstenkorn, S. and Luc, P.: Atlas du spectre d'absorption de la molecule d'iode: 17.500–20.000 cm^{-1}, Laboratoire Aimé Cotton, CNRS II, 91405 Orsay, France, 1977b.

Gerstenkorn, S. and Luc, P.: Atlas du spectre d'absorption de la molecule d'iode: 14.000–15.600 cm^{-1}, Laboratoire Aimé Cotton, CNRS II, 91405 Orsay, France, 1978.

Gerstenkorn, S., Verges, J., and Chevillard, J.: Atlas du spectre d'absorption de la molecule d'iode: 11.000–14.000 cm^{-1}, Laboratoire Aimé Cotton, CNRS II, 91405 Orsay, France, 1982.

Kato, H., Baba, M., Kasahara, S., et al.: Doppler-Free High Resolution Spectral Atlas of Iodine Molecule, Japan Society for the Promotion of Science, 2000.

Kortüm, G. and Friedheim, G.: Lichtabsorption und Molekularzustand des Jods als Dampf und Lösung, Zeitschrift für Naturforschung, 2a, 20–27, 1947.

Marcy, G. W. and Butler, R. P.: Precise Doppler Shifts using an Iodine Cell, PASP, 104, 270–277, 1992.
Ogryzlo, E. A. and Thomas, G. E.: Pressure Dependence of the Visible Absorption Bands of Molecular Iodine, J. Mol. Spectrosc., 17, 198–202, 1965.
Press, W. H., Flannery, B. P., Teukolsky, S. A., and Vetterling, W. T.: Numerical Recipes in C: The Art of Scientific Computing, Cambridge University Press, Cambridge, U.K., 1986.
Rabinowitch, E. and Wood, W. C.: The extinction coefficients of iodine and other halogens, Trans. Faraday Soc., 32, 540–546, 1936.
Richter, A.: Absorptionsspektroskopische Messungen stratosphärischer Spuren-gase über Bremen, 53° N, Cuvillier Verlag, Göttingen, Germany, 1997.
Roscoe, H. K., Johnston, P. V., van Roozendael, M., et al.: Slant Column Measurements of O_3 ad NO_2 during the NDSC Intercomparison of Zenith-Sky UV-Visible Spectrometers in June 1996, J. Atmos. Chem., 32, 281–314, 1999.
Saiz-Lopez, A. and Plane, J. M. C.: Novel iodine chemistry in the marine boundary layer, Geophys. Res. Lett., 31, L04112, doi:10.1029/2003GL019215, 2004.
Saiz-Lopez, A. R., Saunders, W., Joseph, D. M., Ashworth, S. H., and Plane, J. M. C.: Absolute absorption cross section and photolysis rate of I_2, Atmos. Chem. Phys., 4, 1443–1450, 2004, SRef-ID: 1680-7324/acp/2004-4-1443.
Shirley, D. A. and Giauque, W. F.: The entropy of Iodine, Heat Capacity from 13 to 327 K, Heat of Sublimation, J. Am. Chem. Soc., 81, 4778–4779, 1959.
Solomon, S., Schmeltekopf, A. L., and Sanders, W. R.: On the interpretation of zenith sky absorption measurements, J. Geophys. Res., 92, 8311–8319, 1987.
Stule, D. R. (Ed.): Thermochemical Tables, Dow Chemical, Midland, Mich., USA, 1961.
Sulzer, P. and Wieland, K.: Intensitätsverteilung eines kontinuierlichen Absorptionsspektrums in Abhängigkeit von Temperatur und Wellenzahl, Helv. Phys. Acta, 25, 653–676, 1952.
Tellinghuisen, J.: Resolution of the visible-infrared absorption spectrum of I_2 into three contributing transitions, J. Chem. Phys., 58, 2821–2834, 1973.
Vogt, K. and Koenigsberger, J.: Beobachtungen über Absorption in Joddampf und anderen Dämpfen, Zeitschrift für Physik, 13, 292–311, 1923.

Table 1. Spectra were simulated for four different spectroscopic configurations. Differential amplitude was determined from these spectra. Configurations A, C, and D are typical for atmospheric DOAS observations. The expected effects on ΔA_{app} are those which would result, if a reference spectrum obtained at equivalent OD of A(500 nm)≈1.0 were used for DOAS retrieval of low atmospheric column density. The obtained atmospheric column density would be overestimated. Comparing the ratio of FWHM upon $\Delta\lambda$ to the observed effect on ΔA_{app} shows that not binning – i.e. the number of pixels per FWHM – but resolution expressed by FWHM is the major source of this effect.

config.	grating [grves·mm^{-1}]	$\Delta\lambda$ [nm/pixel]	FWHM [nm]	FWHM/$\Delta\lambda$ [pixel]	effect on ΔA_{app}	reference
A	1200	0.035	0.175 (0.25)	5 (7.1)	2%	Saiz-Lopez and Plane (2004) this work
B	600	0.077	0.35	4.5	5%	
C	600	0.077	1.0	13.0	12%	Aliwell and Jones (1997)
D	300	0.154	1.3	8.4	13%	Richter (1997)

Table 2. Comparison of results for the absorption cross section of I_2 at λ=500 nm. The average was obtained by using the inverse squared error of each individual measurement as a weight. The error was determined by error propagation.

σ_{I_2}(500 nm) (10^{-18}cm^2·molec^{-1})	method	
2.20±0.07	vapour pressure	Tellinghuisen (1973)
2.29±0.27	vapour pressure	Saiz-Lopez et al. (2004)
2.25±0.09	independent	Bauer et al. (2004)
2.186±0.021	independent	this work
2.191±0.02		**weighted average**

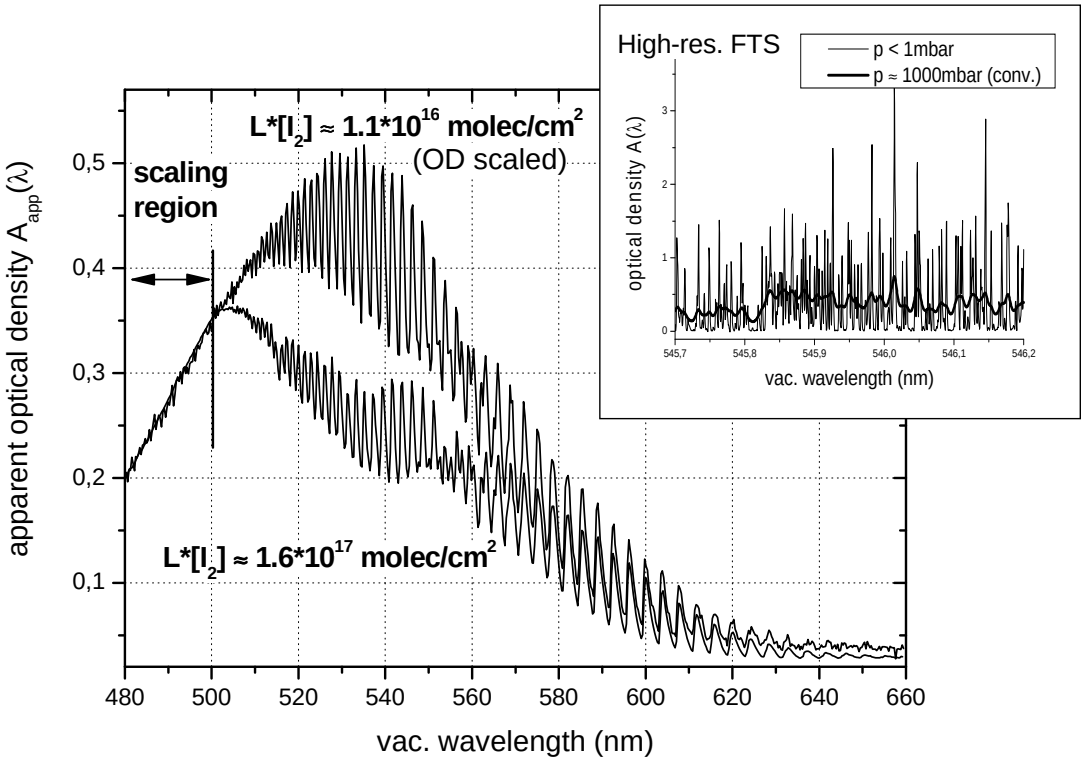

Fig. 1. Two absorption spectra of I_2 were recorded at low resolution. Column density was varied by roughly one order of magnitude between them. The low column density spectrum was scaled to the other in the continuum region at λ<500 nm. In the ro-vibronic region above 500 nm the high column density measurement shows clear sub-linear growth with column density. In the inset graph a section of the high-resolution absorption spectrum of I_2 obtained from Fourier Transform Spectrometer measurements at a resolution of $\approx$0.04 cm^{-1} is shown, courtesy of Marcy and Butler (1992). To simulate atmospheric pressure broadening, the spectrum was convoluted with a 0.3 cm^{-1} Lorentz profile.

ACPD
5, 5183–5221, 2005

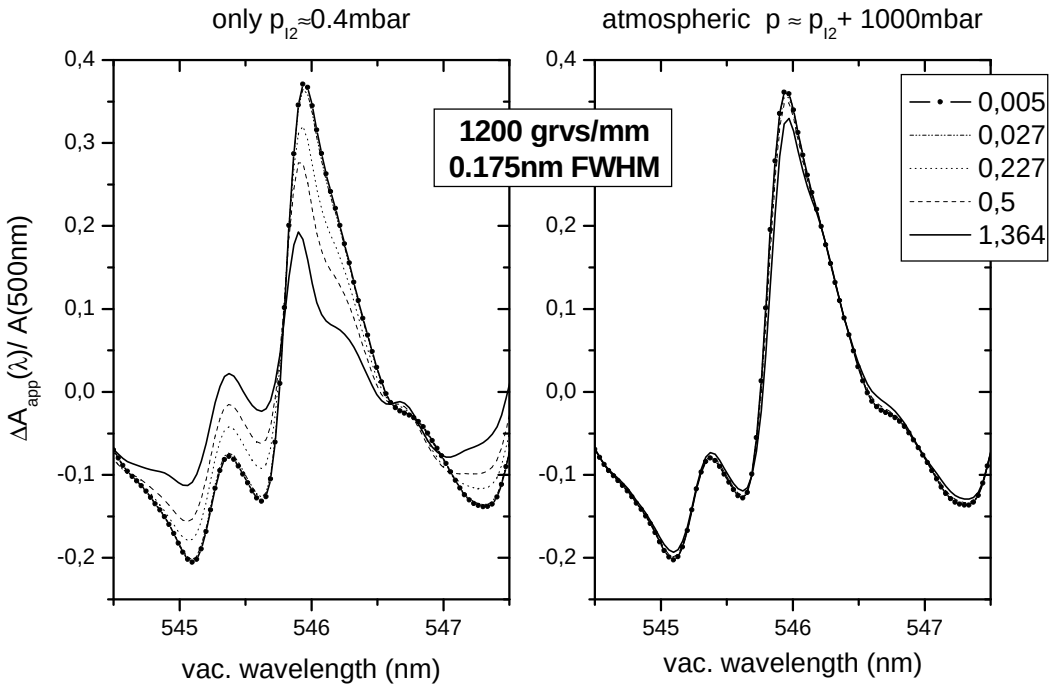

Fig. 2. (a) Based on the high-resolution FTS spectrum of I_2 the apparent differential absorption cross sections were simulated for different column densities of I_2 (see legend: Equivalent OD at 500 nm ranging from 0.005 to 1.364). Shown is the effect on the 546 nm band at low pressure (only I_2, no bath gas, left diagram) and at atmospheric pressure (I_2 plus 1000 mbar of bath gas, right diagram). Increased column density systematically reduces the amplitude of apparent absorption cross sections. The effect is smaller at atmospheric pressure and large at low pressure.

ACPD
5, 5183–5221, 2005

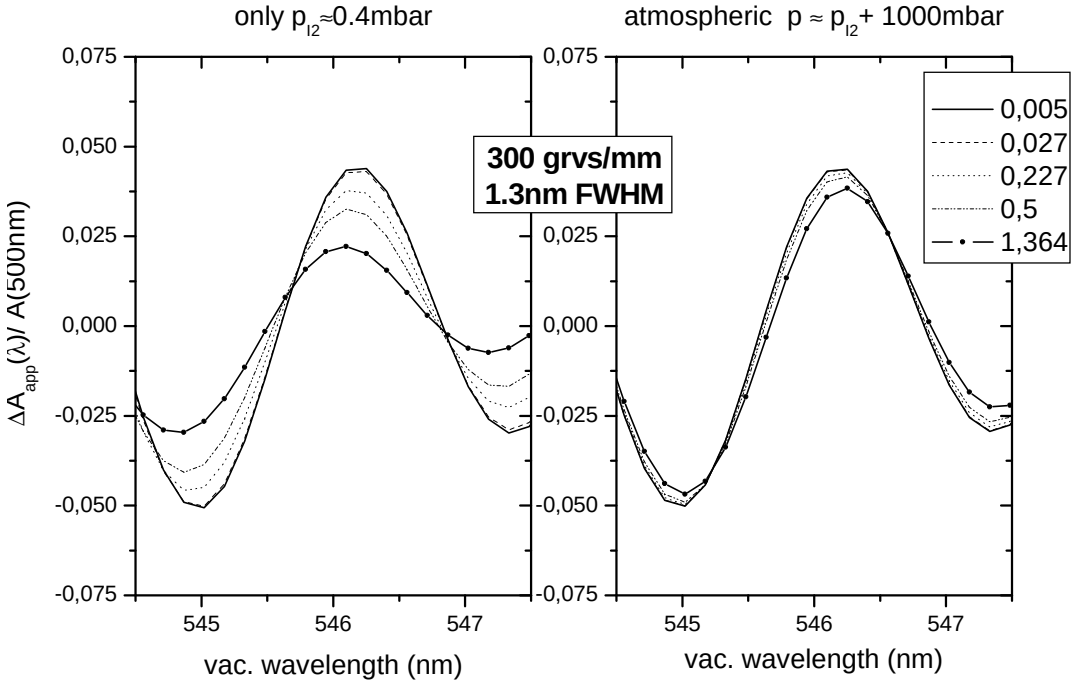

Fig. 2. **(b)** Same as Fig. 2a but for 300 grooves·mm^{-1} and 1.3 nm FWHM. Structures are much more smoothed and the amplitude is reduced relative to the 1200 grooves·mm^{-1} grating spectrum.

ACPD
5, 5183–5221, 2005

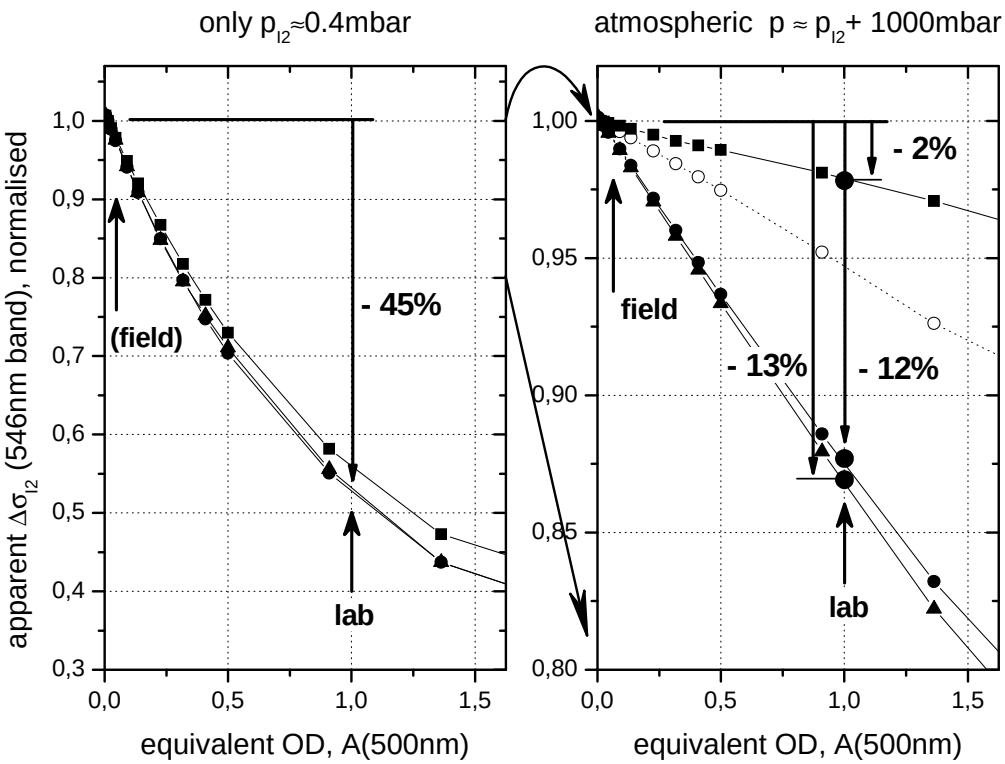

Fig. 3. The amplitude of apparent differential absorption cross section of the 546 nm band was simulated for different spectroscopic conditions and different column densities. Both low pressure (left diagram) as well as atmospheric pressure (right diagram) were considered. The data is plotted against equivalent optical density A(500 nm). Data is normalised to recently observed atmospheric column density of I_2. The effect of using reference spectra obtained at laboratory conditions for DOAS retrieval of low column densities is examined. At atmospheric pressure it leads to reduced apparent $\Delta\sigma$ and thereby to overestimation of atmospheric column densities of up to 13%. Under low pressure conditions, which are possibly relevant in laboratory studies, the overestimation reaches 45%.

ACPD
5, 5183–5221, 2005

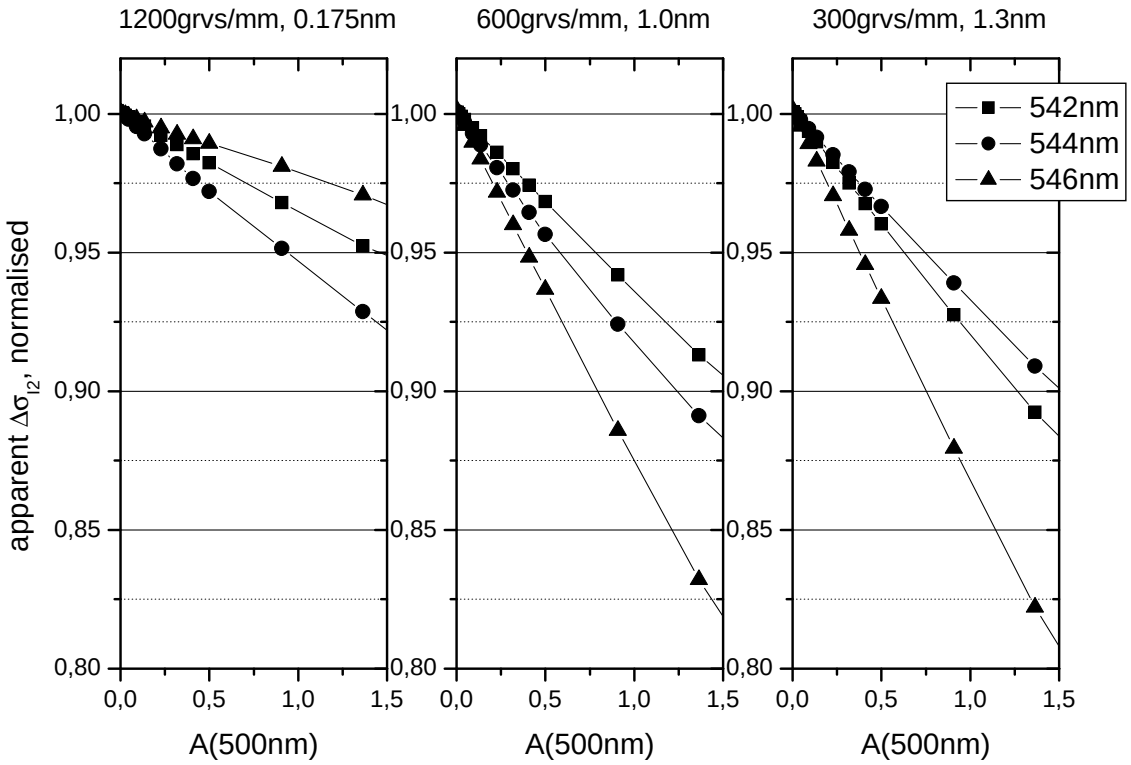

Fig. 4. Sensitivity of different bands to effects of resolution and binning was studied. The amplitude of apparent differential cross section was determined at different bands and under different spectroscopic conditions. It is plotted against equivalent OD at 500 nm, A(500 nm). Clearly sensitivity to resolution is different in different bands. Note the partially mixed order of results obtained from different bands under different conditions.

ACPD
5, 5183–5221, 2005

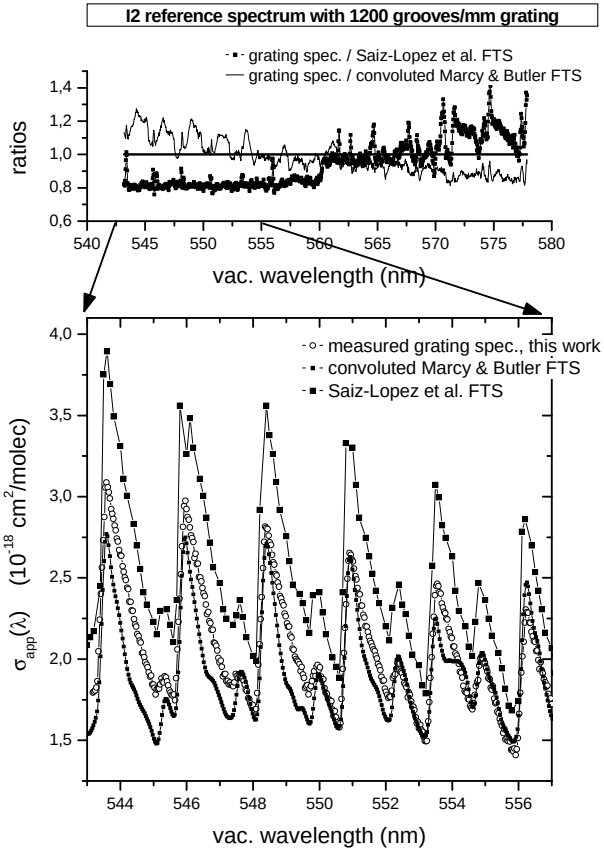

Fig. 5. (a) The spectrum obtained in this work with a 1200 grooves·mm^{-1} grating and 0.25 nm FWHM is compared to a spectrum based on the high-resolution data shown in Fig. 1 simulated for the same spectroscopic conditions as well as to an FTS spectrum obtained by Saiz-Lopez et al. (2004) (0.1 nm step size, 4 cm^{-1} resolution). In the top graph the ratio between our measurement and the latter two compares the systematic deviations between the different spectra.

ACPD
5, 5183–5221, 2005

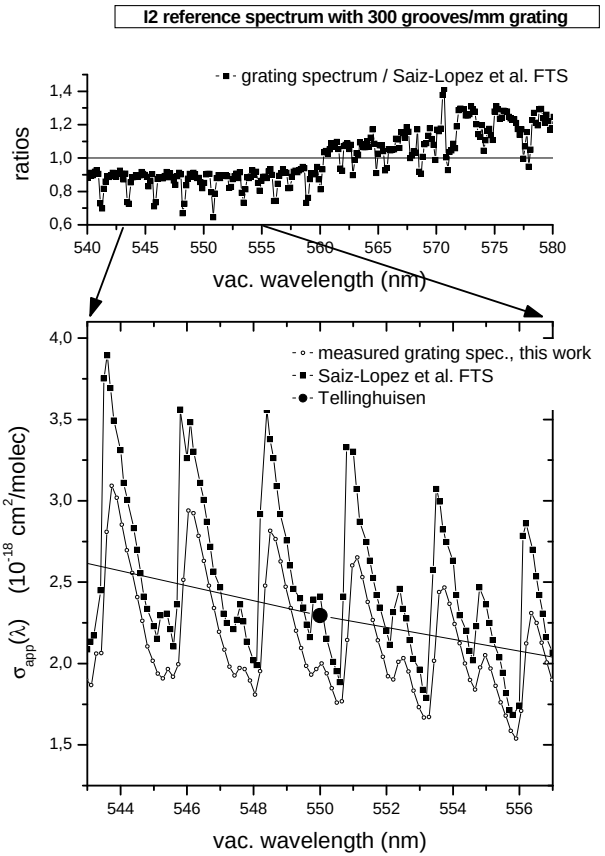

Fig. 5. **(b)** Same as in Fig. 5a, but for the spectrum obtained with a 300 grooves·mm^{-1} grating and 0.59 nm FWHM. The general behaviour of the ratio is the same as between the 1200 grooves·mm^{-1} grating and the FTS spectrum by Saiz-Lopez. The low-resolution data by Tellinghuisen (1973, monochromator: trapezoidal slit function, 2.9 nm base, 2.3 nm peak width) is also plotted for comparison (filled circle).

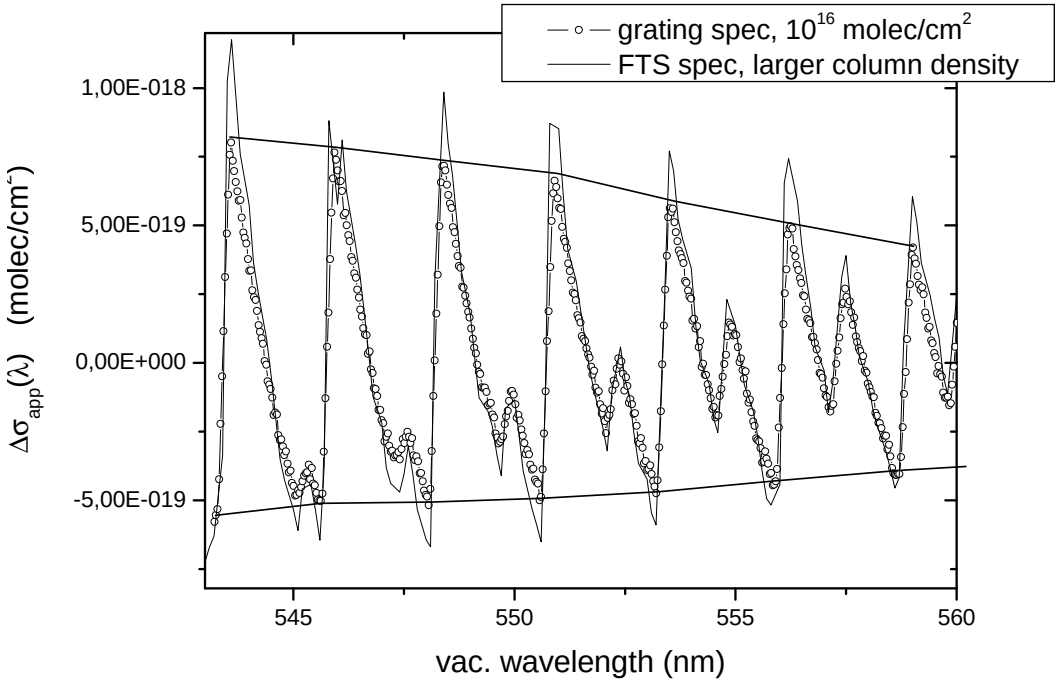

Fig. 6. A spectrum of I_2 was recorded with a 1200 grooves·mm^{-1} grating spectrometer at 0.175 nm FWHM and low column density of 6.9·10^{15} molec/cm^2 (open circles, black line envelope). This is compared to a spectrum recorded with a Fourier Transform Spectrometer at somewhat higher column density (3.1·10^{16} molec/cm^2, 0.1 nm step size, 4 cm^{-1} resolution, solid line). Effects due to different column density are minor. The present deviation in differential amplitude between them of as much as 30% is unresolved and could possibly be attributed to different resolution and different measurement technique.

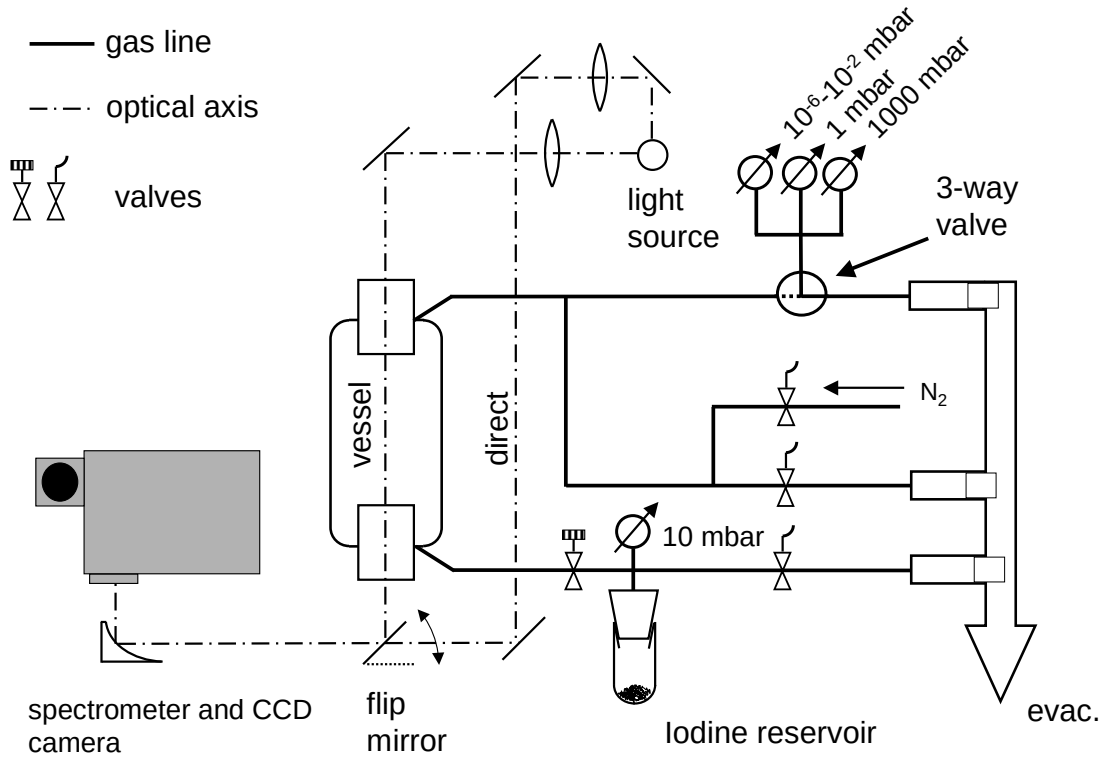

Fig. 7. In the determination of absorption cross section of I_2 simultaneous measurements of OD and pressure were used. Absorption spectroscopy was performed with a Xenon lamp, a spectrometer and CCD camera. A flip mirror enabled near-real time light source monitoring. Pressure in the vessel was automatically monitored with a 0.001 to 1.0 mbar capacitance barometer.

ACPD
5, 5183–5221, 2005

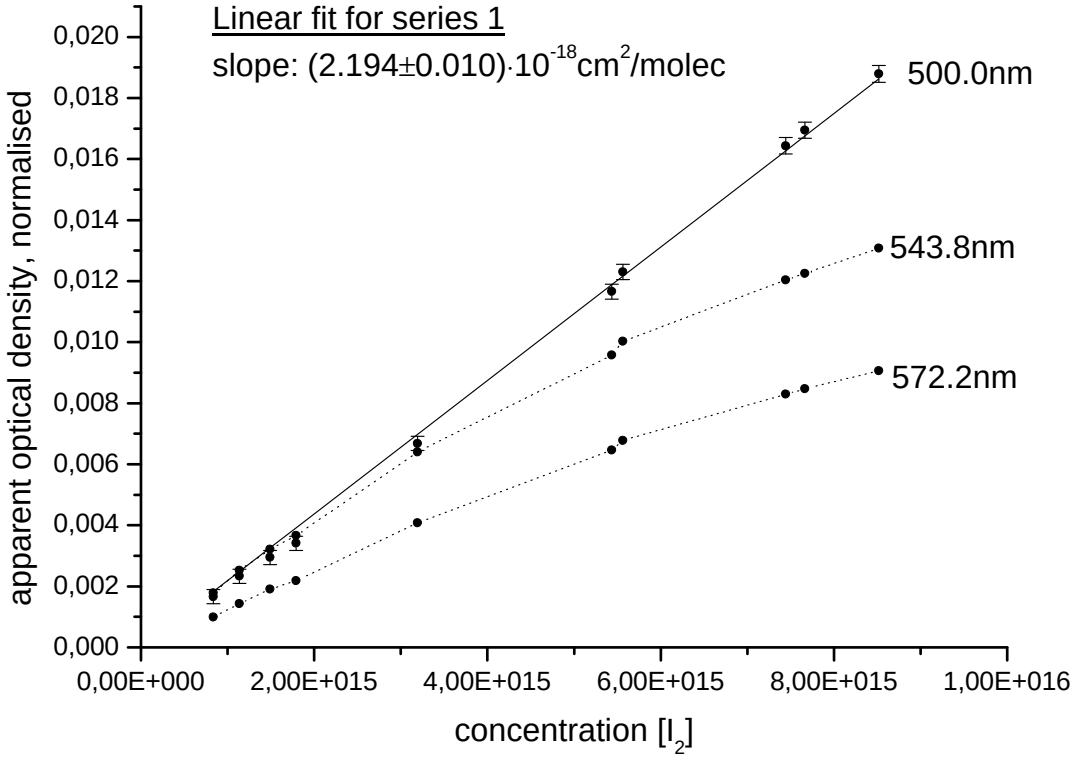

Fig. 8. The absorption cross section of I_2 at 500 nm (air wavelength) in the continuous region of its absorption spectrum was determined by simultaneous spectroscopic and pressure/temperature measurement. The graph shows the linear fit of OD against concentration for the first series of measurements. OD is normalised to unit path length. The linear fit produces the estimate for σ_{I_2}(500 nm). The stated uncertainty is the statistical error estimate from the linear regression, which used uncertainty estimates for both axes. Data for two other wavelengths from the ro-vibronic region (λ>500 nm) is shown, demonstrating the non-linear behaviour of apparent OD in this region due to resolution issues.